Journal of Alloys and Compounds 657 (2016) 495–505

Contents lists available at ScienceDirect

Journal of Alloys and Compounds

journal homepage: http://www.elsevier.com/locate/jalcom

Magnetoresistive and magnetocaloric response of manganite/insulator system

Abd El-Moez A. Mohamed [a, b, *], V. Vega [b, c], M. Ipatov [d], A.M. Ahmed [a], B. Hernando [b]

[a] Physics Department, Faculty of Science, Sohag University, Sohag 82524, Egypt
[b] Physics Department, Faculty of Science, Oviedo University, Oviedo 33007, Spain
[c] Laboratory of Nanoporous Membranes, Oviedo University, Oviedo 33006, Spain
[d] Materials Physics Department, Faculty of Chemistry, Basque Country University, San Sebastian 20018, Spain

ARTICLE INFO

Article history:
Received 12 September 2015
Received in revised form
7 October 2015
Accepted 12 October 2015
Available online 22 October 2015

Keywords:
Grain boundaries
Electrical transport
Magnetoresistance
Magnetization
Entropy
Magnetocaloric effect

ABSTRACT

In this work, we have studied structural, electro-magnetic and magnetocaloric properties of $La_{0.7}Ba_{0.3}MnO_3/xTiO_2$ manganite/insulator system with $0 \leq x \leq 0.08$. X-ray diffraction (XRD) shows the coexistence of TiO_2 and $La_{0.7}Ba_{0.3}MnO_3$ phases in doped composites through their characteristic peaks. This reveals their interaction lack preserving the R-3c rhombohedral structure for all composites. Due to interaction lack, TiO_2 is suggested to segregate at grain boundaries weakening grains connectivity and decreasing metal-semiconductor transition temperature (T_{ms}). The segregated TiO_2 hinders conduction between grains leading to carriers tunneling that increases the low field magnetoresistance (LFMR) of $La_{0.7}Ba_{0.3}MnO_3$ from −3% to −3.3, −3.5 and −3.7% for $x = 0.02$, 0.04 and 0.06 for doped composites. The dc magnetization measurements reveal the constant value of Curie temperature (T_c) and its non impact by doping level referring to the TiO_2–$La_{0.7}Ba_{0.3}MnO_3$ interaction lack. Also, the magnetocaloric properties of $La_{0.7}Ba_{0.3}MnO_3$ are enhanced with TiO_2 doping, where, the relative cooling power (RCP) of $La_{0.7}Ba_{0.3}MnO_3$ has been enhanced from 35 J/kg to 51, 47, 49 and 50 J/kg for $x = 0.02$, 0.04, 0.06 and 0.08 composites at 1.5T magnetic field.

1. Introduction

Magnetoresistive doped manganites interest with several outstanding phenomena associated with their structural, electrical and magnetic properties, as the colossal magnetoresistance (CMR) phenomenon for magnetic recording applications [1] and magnetocaloric effect (MCE) for magnetic refrigeration technology [2]. The electro-magnetic response of these oxides relies on the mixed valence state Mn^{3+}/Mn^{4+} that plays a vital role in the double exchange mechanism (DE), the change in Mn–O–Mn angle and in the e_g electron mobility. So, any disturbance in this ratio may change the electro-magnetic properties. In fact, potential magnetic applications favor the high values of CMR that can be achieved at high magnetic fields, what retard their technological implementation. However, high values of MR have been observed in polycrystalline granular materials and multilayered manganites [3] at low applied magnetic fields (LFMR), pointing to the relevant role of grain boundaries. This discovery has increased the interest in grain boundaries synthesis and their modification either by annealing process [4], preparation methods [5] or artificial defects [6]. The LFMR has been studied carefully and attributed to spin polarized tunneling and scattering mechanisms across grain boundaries according to the polarization ability [7].

Another important property of manganites is the MCE that used in magnetic cooling technology as an alternative to gas compression mode [8]. In magnetic materials, the MCE arises from the change in lattice magnetic entropy (ΔS) as a result of magnetic field application. The applied magnetic field orients the unpaired spins lowering their entropy, this is compensated by an increase in lattice entropy (ΔS) that leads to heat releasing. As spin orientation reaches maximum at T_c under an applied magnetic field, so, ΔS is expected to show a maximum at the same temperature too. With this property, manganites have been explored for magnetic refrigeration applications and found to be good candidates as $La_{0.67}Ba_{0.22}Sr_{0.11}Mn_{1-x}Ti_xO_3$ [9] and $Pr_{0.5}Eu_{0.1}Sr_{0.4}MnO_3$ [10]. This is because of the high

* Corresponding author. Physics Department, Faculty of Science, Oviedo University, Oviedo 33007, Spain.
E-mail address: abdmoez_hussien@science.sohag.edu.eg (A.A. Mohamed).

http://dx.doi.org/10.1016/j.jallcom.2015.10.095
0925-8388/

magnetization, the high T_c, the chemical stability, the simple preparation methods, the low cost and the negligible magnetic hysteresis advantages that have put manganites in comparison with the high MCE Gd [11] and Gd based alloys [12]. For example, $La_{0.7}Ca_{0.3}MnO_3$ shows a MCE response of 5.27 J/kg.K at 1.5T magnetic field, nearly twice larger than Gd based alloys at low magnetic fields [13].

Manganite/insulator system is an inhomogeneous system consists of manganite and insulator materials. This system is characterized by the interaction lack between compounds that keeps the intrinsic properties of the manganite material. Therefore with this system, we can make use of the spin polarized properties and the heterogeneous granular advantages, where, the secondary insulating phase works as an energy barrier at grain boundaries and hinders conduction between grains leading to the spin tunneling and the LFMR. This work has two important aims, first one is the attempt to enhance the LFMR of $La_{0.7}Ba_{0.3}MnO_3$ (LBMO) by the artificial boundaries, this is by introducing TiO_2 insulator as a secondary phase forming LBMO/xTiO$_2$ system. The second aim is to explore the magnetocaloric properties of this system, which are expected to be promising because we talking about a change in the MCE properties at the same temperature range (T_c).

2. Experimental method

LBMO/xTiO$_2$ ceramic samples with x = 0, 0.02, 0.04, 0.06 and 0.08 were prepared in several steps. LBMO was prepared by the sol–gel method using $LaN_3O_9.6H_2O$, $Ba(OOCCH_3)_2$ and $Mn(OOCCH3)_2$ $.4H_2O$ starting raw compounds. Stoichiometric solutions of these salts were mixed and stirred together, then 1:1 volume ratio of citric acid was added during the stirring process and resulted in a white colloid. After drying, the brown xerogel was ground and calcined at 600 °C for 8 h. The obtained black powder was pressed and sintered at 1200 °C for 24 h. TiO_2 nanotubes (NTs) were prepared by the electrochemical anodization method as reported in [14], where Ti foils with high purity (99.6%) were cleaned ultrasonically in acetone, isopropanol, ethanol and de-ionized water, respectively. The anodization process was carried out at room temperature for 24 h in electrochemical cell with platinum grid cathode at constant dc voltage (60 V). The electrolyte solution was a mixture of ammonium fluoride (0.3%), ethylene glycol and de-ionized water (1.8%). The resultant TiO_2 NTs were calcined at 400 °C for 2 h to increase their crystallinity obtaining the anatase phase [15]. Finally, stoichiometric amounts of LBMO and TiO_2 NTs were mixed, pelletized and sintered at 800 °C for 24 h.

The crystal structure was examined by XRD at room temperature and the structural information was obtained by Rietveld refinement using FULLPROF program. The surface morphology was carried out using scanning electron microscope (SEM). Electrical resistivity measurements in zero and 0.5T magnetic field were measured by the standard four-point Van der Pauw technique, and the magnetic measurements were performed using SQUID magnetometer.

3. Results and discussion

3.1. Structure

XRD patterns in Fig. 1a show the single phase of LBMO with additional peaks of TiO_2 in doped composites at $2\theta = 25.32°$ and 48.25°. The coexistence of TiO_2 with the LBMO phase in all doped composites suggests their interaction lack that preserves the R-3c rhombohedral structure of LBMO with doping level as

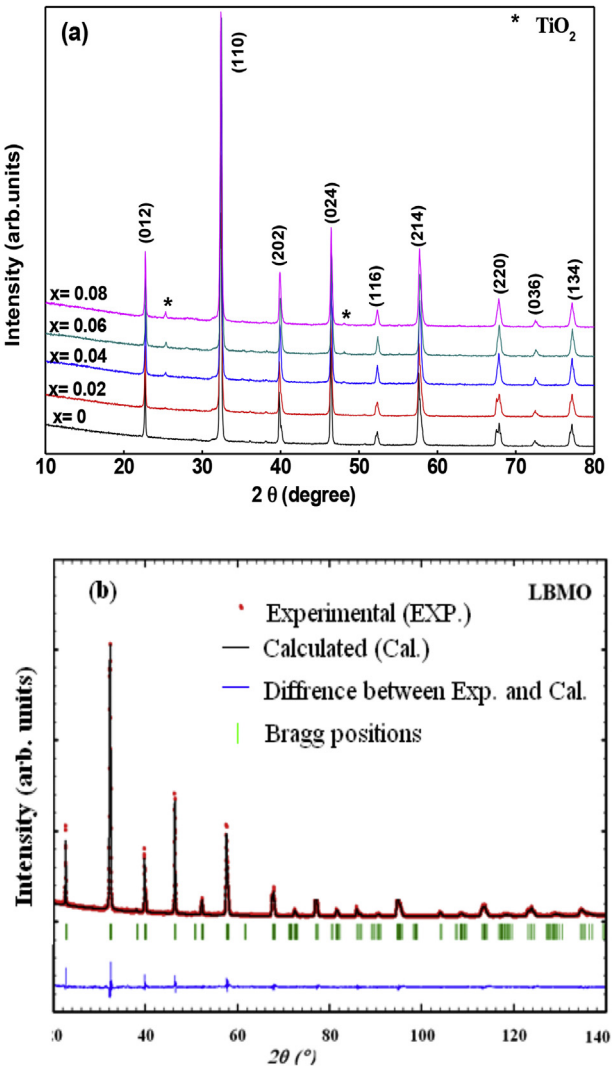

Fig. 1. (a) XRD patterns of LBMO/xTiO$_2$ composites, $0 \leq x \leq 0.08$ and (b) Rietveld based calculated profile of the undoped compound LBMO.

proved by Reitveld refinement. Where, Fig. 1b shows Reitveld profile for LBMO compound as an example with refinement factors listed in Table 1 as the goodness of fitting (χ^2), the crystallographic factor (R_F) and the Bragg factor (R_B). TiO_2–LBMO interaction lack may be supported by SEM micrographs, where, Fig. 2 shows TiO_2 NTs destruction, during preparation process, and their precipitation at the boundaries and on the surfaces of LBMO as segregated grains. This explains the insignificant change in cell volume, lattice constants (a, c), SEM grain size and structure stability with increasing doping level as seen in Table 1. Moreover, the presence of La, Ba, Mn and Ti elements were confirmed for the nominal composition by the energy dispersive

Table 1
Lattice constants, cell volume (V), SEM grain size and Rietveld agreement factors for LBMO/xTiO$_2$.

Composition	a(Å)	c(Å)	V(Å)^3	Grain size (μm)	χ^2	R_f	R_B
x = 0	5.54368	13.483	358.86	0.748	3.12	5.44	5.30
x = 0.02	5.54093	13.483	358.52	0.659	2.65	3.12	3.02
x = 0.04	5.5349	13.503	358.25	0.659	3.39	4.04	3.35
x = 0.06	5.5347	13.503	358.20	0.684	5.39	4.59	4.13
x = 0.08	5.5360	13.497	358.22	0.635	2.85	4.60	3.98

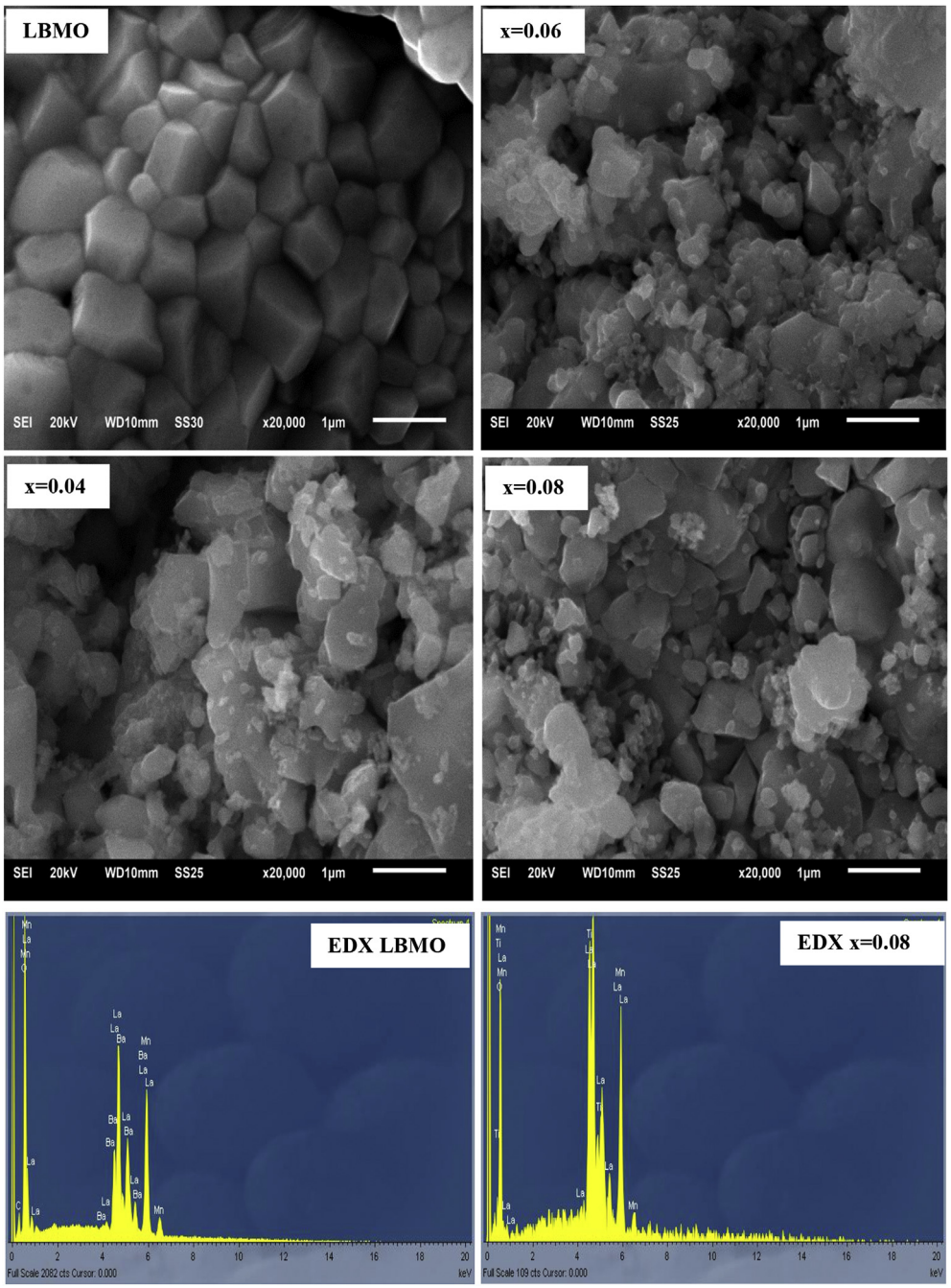

Fig. 2. SEM of LBMO, x = 0.04, x = 0.06 and x = 0.08, and the EDX of LBMO and x = 0.08 composites.

X-ray (EDX) analysis, where, their characteristic peaks are clearly observed in the spectra as shown in Fig. 2.

3.2. Transport properties

Fig. 3 shows the temperature dependence of zero field resistivity curves, ρ(T), of LBMO/xTiO$_2$ composites. As common in Ba and small grain size manganites [16–19], LBMO shows a double-peak resistivity at T_{p1} and T_{p2} temperatures as shown in the inset of Fig. 3. T_{p2} represents the real T_{ms} and ascribed to the DE interaction between Mn^{3+} and Mn^{4+} ions (Mn^{3+}–O–Mn^{4+}) [20] that is responsible for the metallic behavior below this temperature. Whereas, T_{p1} reflects the interfacial tunneling effect at grain boundaries [21] that arises from the difference in magnetic ordering between the surface and the core of the grain. With increasing doping level, the resistivity increases and the T_{ms} decreases with a discontinuity at x = 0.04 (see Table 2) in agreement with [22–24].

To explain doping effect on the transport properties, we will consider the grain effects (size and distribution), but as observed in Table 1, the negligible change in grain size suggests to consider only the effect of grain distribution. Conduction in granual manganites occurs through the direct contact between grains that work as conduction channels [25]. Therefore, it is expected to get two different kinds of conduction channels in our system. The main conductive channels of LBMO grains responsible for

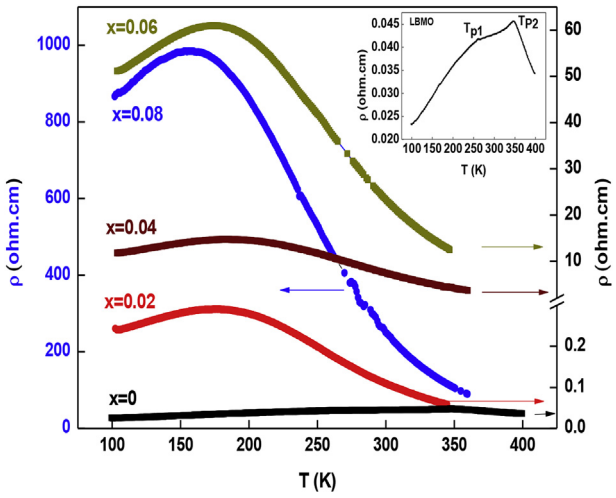

Fig. 3. Temperature dependence of zero field resistivity for LBMO/xTiO$_2$ composites and the inset shows a clear vision of the undoped LBMO compound.

the properties and the secondary insulating channels of TiO_2 grains, which are distributed at the boundaries and on the surfaces of LBMO grains. Accordingly, the change in the transport properties can be understood depending on the interruption of LBMO conduction by the additive TiO_2. The segregated TiO_2 weakens the connectivity of LBMO grains and increases their boundaries resistance leading to conduction interruption, which in turn increases resistivity and decreases T_{ms} with TiO_2 content [22,26]. The increase in grain boundaries resistance with TiO_2 doping can be inferred by the increase in low temperature resistivity (ρ_{100K}) that mainly origins from grain boundaries (see Fig. 3 and Table 2). The discontinuity behavior of T_{ms} at $x = 0.04$ may refer to the TiO_2 agglomeration as interstitial grains between LBMO grains opening new conductive parallel channels [23], in agreement with [24,27]. Also, it is noteworthy the larger increase in resistivity at $x \geq 0.06$ composites that may be attributed to a small partial substitution of Mn^{3+} ions by Ti^{4+} ions in LBMO lattice that promotes resistivity with an intrinsic factor. The Mn^{3+} partial substitution suppresses the ferromagnetic DE interactions due to the non-participation of Ti^{4+} in this mechanism (Mn^{3+}–O–Ti^{4+}). In addition, the difference in ionic size between Ti^{4+} (0.605 Å) and Mn^{3+} (0.66 Å) leads to LBMO lattice distortion that decreases Mn–O–Mn angles and hence decreases e_g electron mobility. In general, both consequences of Mn^{3+} partial substitution result in a stronger localization of e_g electron and a larger increase in resistivity of $x \geq 0.06$ composites. The Mn^{3+} partial substitution suggestion at $x \geq 0.06$ composites may be acceptable because of the small change in T_c at $x = 0.08$ composite as will be seen in the magnetic measurements.

To recognize conduction mechanism nature above and below T_{ms}, resistivity data were analyzed with well established models and experimental equations in each region. In the semiconducting region, above T_{ms}, resistivity data were examined using the small polaron hopping (SPH) and the variable range hopping (VRH) models. The SPH model with $\rho/T = \rho_\alpha \exp(E_\rho/k_BT)$ formula [28] is well applicable at $T > \theta_D/2$ as shown in Fig. 4a, where ρ_α is a constant, $\mathbf{E_\rho}$ is the activation energy at high temperatures, $\mathbf{k_B}$ is Boltzmann constant, θ_D is Debye temperature and $\theta_D/2$ is the deviation temperature of linearity with this model. While, the VRH model with expression $\sigma = \sigma_0 \exp(-T_0/T)^{1/4}$ [28] is well fitted with the resistivity data at $T_{ms} < T < \theta_D/2$ as shown in Fig. 4b, where $T_0 = 18/k_BN(E_F)a^3$ is the Mott characteristic temperature, $\mathbf{N(E_F)}$ is the density of states near Fermi level (E_F) and $\boldsymbol{a}$ is the localization length and equals 0.45 nm as reported in Ref. [29]. And according to the VRH model, at $T_{ms} < T < \theta_D/2$ carriers can hop from site to site with hopping energy E_h passing a distance R_h, which are temperature dependent parameters and can be determined from $E_h(T) = 1/4k_BT^{3/4}T_0^{1/4}$ and $R_h(T) = 3/8a(T_0/T)^{1/4}$ equations [30]. The continuous increase in grain boundaries thickness and resistance with doping level increases carriers hopping distance (R_h) and localization, which decreases $N(E_F)$ and transport across grains (see Table 2). So, carriers need more energy to overcome barriers and localization for easy transport between grains, what explain the monotonic increase of E_ρ and E_h with TiO_2 content in Table 2, in agreement with [4]. Also, the promotion of LBMO carriers localization with TiO_2 addition increases its SPH temperature range that could be inferred by the decrease in θ_D and phonon frequency (υ_{Ph}) values as seen in Table 2 (υ_{Ph} has been determined from $h\upsilon_{Ph} = k_B\theta_D$ relation, and h is Planck constant).

On the other hand, resistivity data in the metallic region, below T_{ms}, were examined by empirical equations Eqs. (1–4). Where, $\boldsymbol{\rho_0}$ is the resistivity arises from the grain boundaries component and temperature independent parameters, $\boldsymbol{\rho_2T^2}$ term arises from the electron–electron interactions, $\boldsymbol{\rho_{2.5}T^{2.5}}$ term arises from the electron–magnon interactions, $\boldsymbol{\rho_{4.5}T^{4.5}}$ term arises from the spin wave scattering process and $\boldsymbol{\rho_5T^5}$ arises from the electron–phonon interactions. The resistivity data of LBMO satisfy Eq. (4), as seen in Fig. 4c. This exhibits the roles of grain boundaries, electron–electron interaction, spin wave and electron–phonon interactions in conduction mechanism at this compound. But in doped composites, the resistivity data are fitted more with Eq. (3) as shown in Fig. 4d. This excludes electron–phonon interactions conduction participation in doped composites because of the increase in scattering process due to the presence of TiO_2 as scattering centers. Generally, Table 3 confirms that grain boundaries component has the most effective role in resistivity change with doping level that supports the experimental results.

$$\rho = \rho_0 + \rho_2T^2 \quad (1)$$

$$\rho = \rho_0 + \rho_{2.5}T^{2.5} \quad (2)$$

$$\rho = \rho_0 + \rho_2T^2 + \rho_{4.5}T^{4.5} \quad (3)$$

Table 2
T_{ms} (K), T_c (K), ρ_{100K} (Ω.cm), MR_{100K} (%), SPH and VRH parameters for LBMO/xTiO$_2$ composites.

	T_{ms}(K)	T_c(K)	θ_D (K)	υ_{Ph} (Hz)	E_ρ(mev)	N(E_F) (eV^{-1} Cm^{-3})	R_h (Å) $_{300\ K}$	E_h(mev) $_{300\ K}$	$\rho_{100\ K}$ (Ω.cm)	$MR_{100\ K}$ (%)
x = 0	350	348	716.84	1.49×10^{13}	110.02	20.44×10^{20}	13.19	50.56	0.023	−11.19
x = 0.02	179	348	560	1.16×10^{13}	136.96	7.14×10^{20}	17.15	65.77	0.24	−15.49
x = 0.04	186	348	589	1.22×10^{13}	139.49	6.06×10^{20}	17.87	68.51	11.6	−15.54
x = 0.06	174	348	571	1.19×10^{13}	142.18	4.77×10^{20}	18.97	72.72	50.97	−12.89
x = 0.08	163	346	568	1.18×10^{13}	176.87	3.45×10^{20}	20.44	78.38	864.5	−9.08

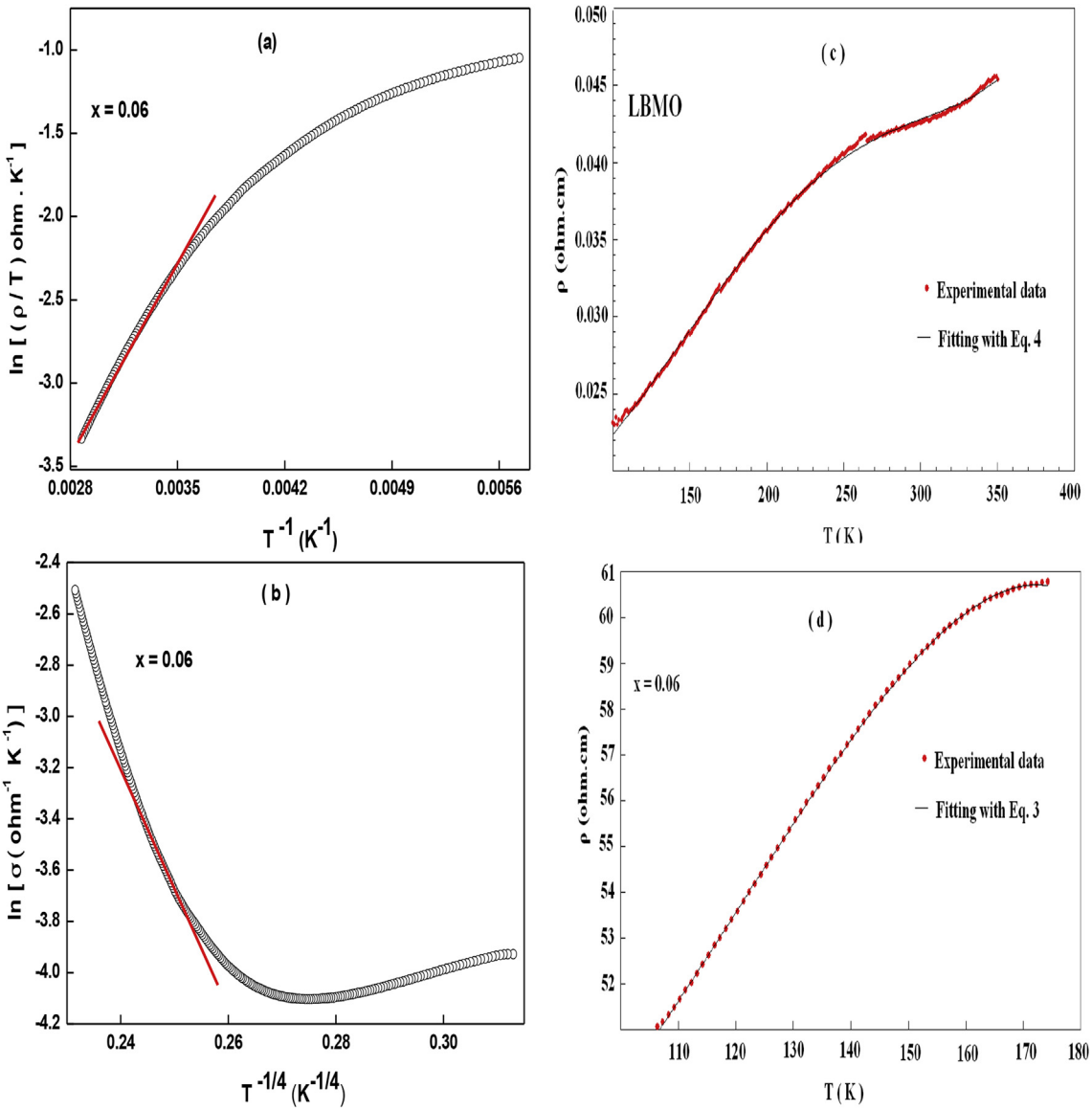

Fig. 4. (a) SPH and (b) VRH models for x = 0.06 composite, and the red solid line represents the best fitted points with these models, while (c) and (d) are the fitting of resistivity below T_{ms} with Eq. (4) and Eq. (3) for LBMO and x = 0.06 respectively.

$$\rho = \rho_0 + \rho_2 T^2 + \rho_{4.5} T^{4.5} + \rho_5 T^5 \quad (4)$$

Fig. 5 shows the temperature dependent MR, which has been calculated from **[ρ(H)−ρ(0)]/ρ(0)** equation, where, **ρ(H)** is the resistivity measured in 0.5T magnetic field and **ρ(0)** is the resistivity measured in zero magnetic field. In this figure, composites with x ≤ 0.04 show a negative MR all over the temperature range, while, x ≥ 0.06 composites show a crossover from negative to positive MR in a plunge at relatively high temperatures, which is quite familiar in some manganites [22,31]. The negative MR has a high value at low temperatures decreases with temperature elevation and passes through peak, in similar behavior with [32]. LBMO shows a MR peak at temperature close to its T_{ms} with a maximum of −3% that is shifted towards lower temperatures with TiO_2 doping and increases in value to −3.3, −3.5 and −3.7% for x = 0.02, 0.04 and 0.06, respectively. Table 2 also shows the low temperature MR value (at 100 K) with TiO_2 doping as an evidence of the general enhancement. The LFMR enhancement with doping level at x ≤ 0.06 refers to the increase in grain boundaries resistance leading to scattering and spin-polarized tunneling across the insulating grains [3,7]. While, with further doping amounts (x = 0.08), the grain boundaries resistance and thickness may exceed the spin memory length [33] decreasing electron tunneling effect, which in turn decreases the LFMR [34].

The negative or positive sign of MR is mainly related to the majority and minority spin carriers, respectively, near E_F [35], suggesting spin carriers change at x ≥ 0.06. In more details, due

Table 3
The best-fitting parameters in the ferromagnetic region obtained from the experimental Eq. (3) and Eq. (4) for all composites.

Composition	ρ_0	ρ_2	$\rho_{4.5}$	ρ_5
x = 0	0.0145	7.53×10^{-7}	-1.11×10^{-12}	4.7×10^{-14}
x = 0.02	0.166	2.26×10^{-7}	-2.41×10^{-13}	–
x = 0.04	8.32	3.19×10^{-4}	-2.94×10^{-10}	–
x = 0.06	37.37	1.35×10^{-3}	-1.45×10^{-9}	–
x = 0.08	638.97	2.48×10^{-2}	-3.53×10^{-8}	–

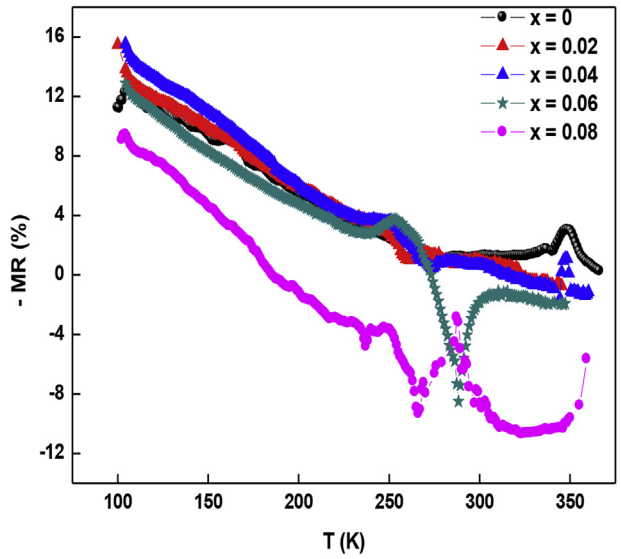

Fig. 5. Temperature dependence of magnetoresistance for LBMO/xTiO$_2$ composites.

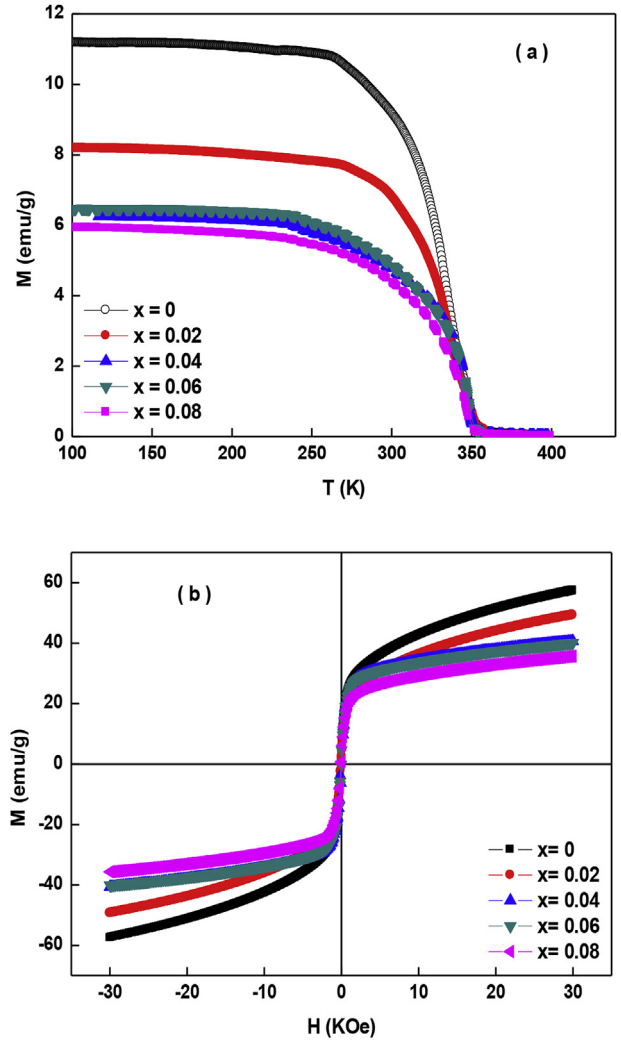

Fig. 6. (a) Temperature dependence of magnetization at H = 100 Oe and (b) Hysteresis loop at 300 K for LBMO/xTiO$_2$ composites.

to the complete TiO$_2$–LBMO interaction lack at x ≤ 0.04, Ba^{2+} electrons will keep occupying the e_g band of LBMO representing the major spin carriers near E_F that exhibits a negative MR. While at x ≥ 0.06, the small partial substitution of Mn^{3+} by Ti^{4+} may result in Ti^{4+} electrons leakage into LBMO leading to the spin carriers change and hence the change in MR sign. Where at low temperatures of x ≥ 0.06, Ti^{4+} electrons go to occupy e_g band ($e_g^{\downarrow}$ or $e_g^{\uparrow}$ state) of LBMO preserving the majority carriers spins that exhibits a negative MR [35]. Whereas with temperature elevation, Ti^{4+} electrons start to occupy the $t_{2g}^{\downarrow}$ band, where its edge becomes closer to the E_F than the e_g band. In this case, the spin orientation of $t_{2g}^{\downarrow}$ becomes antiparallel with the system leading to the minority spin carriers near E_F and the positive MR [35].

3.3. Magnetization

Fig. 6a shows the temperature dependence of dc magnetization, M(T), at 100 Oe magnetic field, where, the ferromagnetic-paramagnetic (FM-PM) transition characterizes all composites at T_c. The sharp drop in the magnetic transition of LBMO ensures its high homogeneity as observed in XRD, while, the relative broadness of magnetic transition in doped composites refers to the TiO$_2$ presence as an impurity phase [36]. TiO$_2$ doping is found to decrease system's magnetization due to the decrease in LBMO ferromagnetic ratio. The magnetic transition temperature, T_c, was determined from the minimum of dM/dT curves and is listed in Table 2. This table shows the T_c independency of doping content, where it shows a constant value of 348 K for all composites with insignificant change at x = 0.08, in agreement with [37,38]. The non impact of T_c by TiO$_2$ doping level refers to its intrinsic property that depends on the ferromagnetism inside the grain [39]. Where, TiO$_2$ affects the grain boundaries only, due to TiO$_2$–LBMO interaction lack, without any change in the grain ferromagnetism or T_c. In the same way, the insignificant change of T_c at x = 0.08 can be easily understood, where, the small partial substitution of Mn^{3+} by Ti^{4+} weakens the intrinsic grain ferromagnetism through the antiferromagnetic Mn^{3+}-O-Ti^{4+} bonds that decreases T_c. In contrast, T_{ms} is an extrinsic property can be easily affected by grain boundaries, so, the occurrence of T_{ms} far below T_c [39,40] is reasonable and shows up the grain boundaries role as a main source of resistivity rather than the grain itself [41]. Fig. 6b shows the hysteresis loops at 300 K, and the narrow hysteresis characterizes all composites. This figure shows the rapid increase in magnetization at low magnetic fields and the tendency of saturation at high magnetic fields. The saturation magnetization decreases with doping level as a result of ferromagnetism ratio dilution and the non magnetic nature of TiO$_2$.

3.4. Magnetocaloric effect (MCE)

The isothermal magnetization curves as a function of magnetic field, with $\mu_0 H = 0–3T$ and thermal interval 5 K, are shown in Fig. 7. Below T_c, magnetization increases sharply with low magnetic fields and saturates at high magnetic fields corresponding to the ferromagnetic behavior. While above T_c, magnetization increases linearly with the applied magnetic field indicating the paramagnetic behavior. The FM-PM transition nature has been determined using Arrott's plots in Fig. 8, where, the positive slope of these plots around T_c indicates the second order transition [42]. Gibbs's free energy in Eq. (5) also can provide another proof for the second order transition, where the positive value of the thermodynamic parameter b(T_c) in Fig. 9 is the condition of the second order transition [43,44], b(T) has

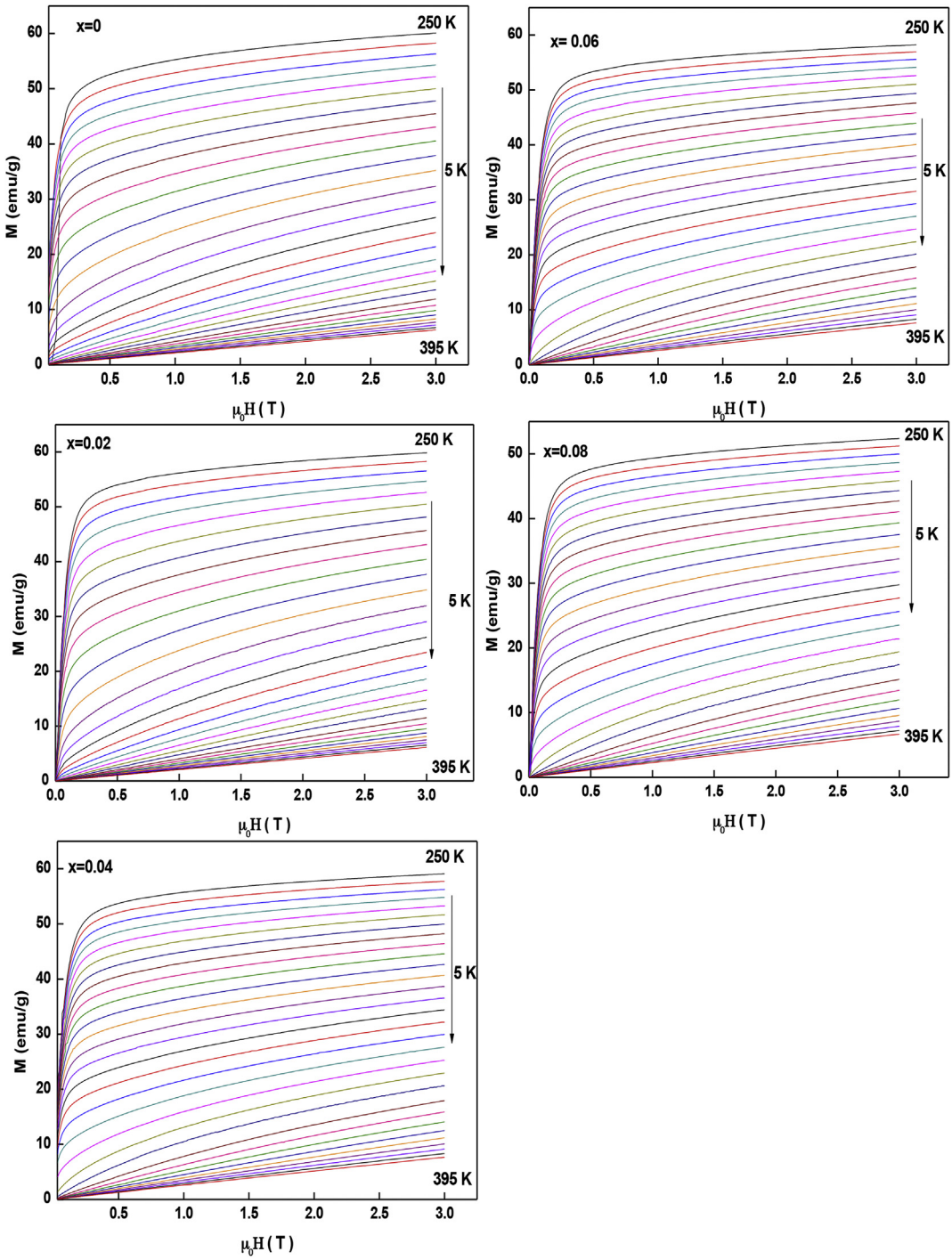

Fig. 7. Isothermal magnetization curves at different temperatures of LBMO/xTiO$_2$ composites.

been determined from Eq. (6) (the equilibrium state of Eq. (5) at $\delta G/\delta M = 0$).

$$G(M,T) = G_0 + \frac{a(T)}{2}M^2 + \frac{b(T)}{4}M^4 + \frac{C(T)}{6}M^6 + \ldots\ldots\ldots - \mu_0 H \quad (5)$$

$$\mu_0 H = a(T)M + b(T)M^3 + C(T)M^5 \quad (6)$$

$$\Delta S(T,\Delta H) = \sum \frac{M_i - M_{i+1}}{T_i - T_{i+1}}\ \Delta H \quad (7)$$

The MCE based on the magnetic entropy change, ΔS, was determined from the isothermal magnetization curves using the approximated Maxwell's relation in Eq. (7) [45]. Where, M_{i+1} and M_i are the magnetization values measured at T_{i+1} and T_i temperatures in magnetic field ΔH. The thermal variation of ΔS at different applied magnetic fields is shown in Fig. 10, where, ΔS shows negative values with a maximum (ΔS_{max}) around T_c that increases in value with the applied magnetic field. Fig. 11 shows the decrease in ΔS_{max} value and the insignificant change in its temperature position with doping level. This decrease in value is

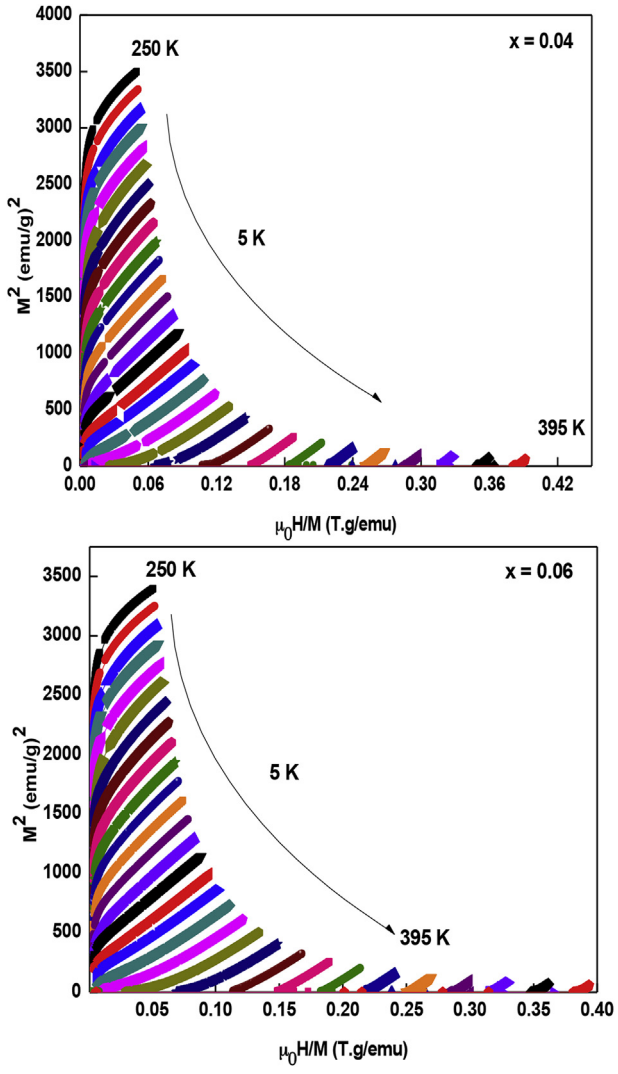

Fig. 8. Arrott's plots for x = 0.04 and x = 0.06 composites as selected samples.

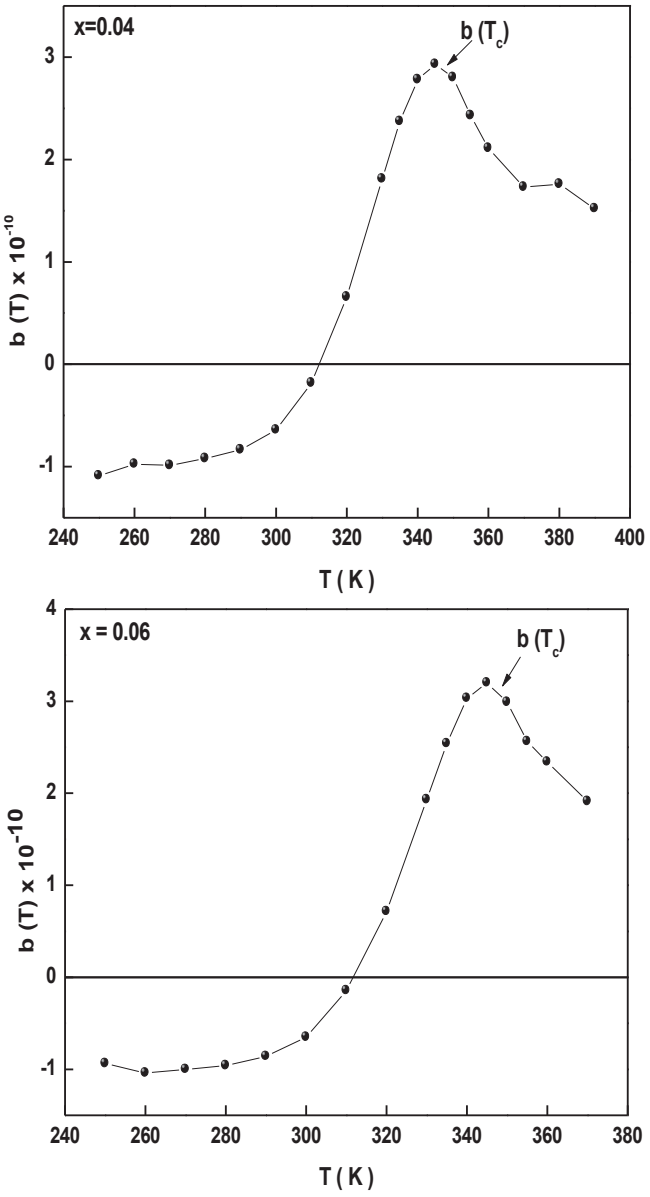

Fig. 9. Thermal variation of b(T) parameter for x = 0.04 and x = 0.06 composites.

attributed to the decrease in the LBMO ferromagnetic ratio with doping level, while, the negligible change in position refers to the constant T_c. The efficient MCE material should have a high value of ΔS and at a wide temperature range. So, depending on these two parameters, the magnetic cooling efficiency of our samples can be determine in terms of the relative cooling power (RCP) in Eq. (8) [46], where, δT_{FWHM} is the full width at half maximum of ΔS curve.

$$RCP = \Delta S_{Max} \times \delta T_{FWHM} \quad (8)$$

In spite of the decrease in ΔS_{Max} with doping level, as discussed before, but TiO_2 doping is found to increase the spread of MCE temperature range, which can be inferred by the increase in δT_{FWHM} as seen in Table 4. So, the δT_{FWHM} increase is responsible for the notable enhancement in RCP values with doping level as shown in Table 4 and so with the applied magnetic fields ≥ 1T as shown in Fig. 12. In Table 4, we present a comparison between our system and other works in the magnetocaloric properties, this comparison suggests the applicability of system in low field-high temperature magnetic refrigeration applications.

From the MCE measurements, we can draw an interesting feature of the *manganite/insulator* system that is related to the RCP variation in the same temperature range. In more details, ΔS shows a maximum around T_c and any attempt to enhance this value by substitution process with other element results in a change in the T_c, which in turn changes the RCP working temperature range. But, this is rarely happen in the *manganite/insulator* system because of the interaction lack between the insulator and the manganite material that preserves T_c of the manganite material at the same value that keeps the same RCP temperature range. By this way, if we could choose a manganite material with an optimum T_c especially in room temperature range, we might enhance the MCE properties without changing this temperature.

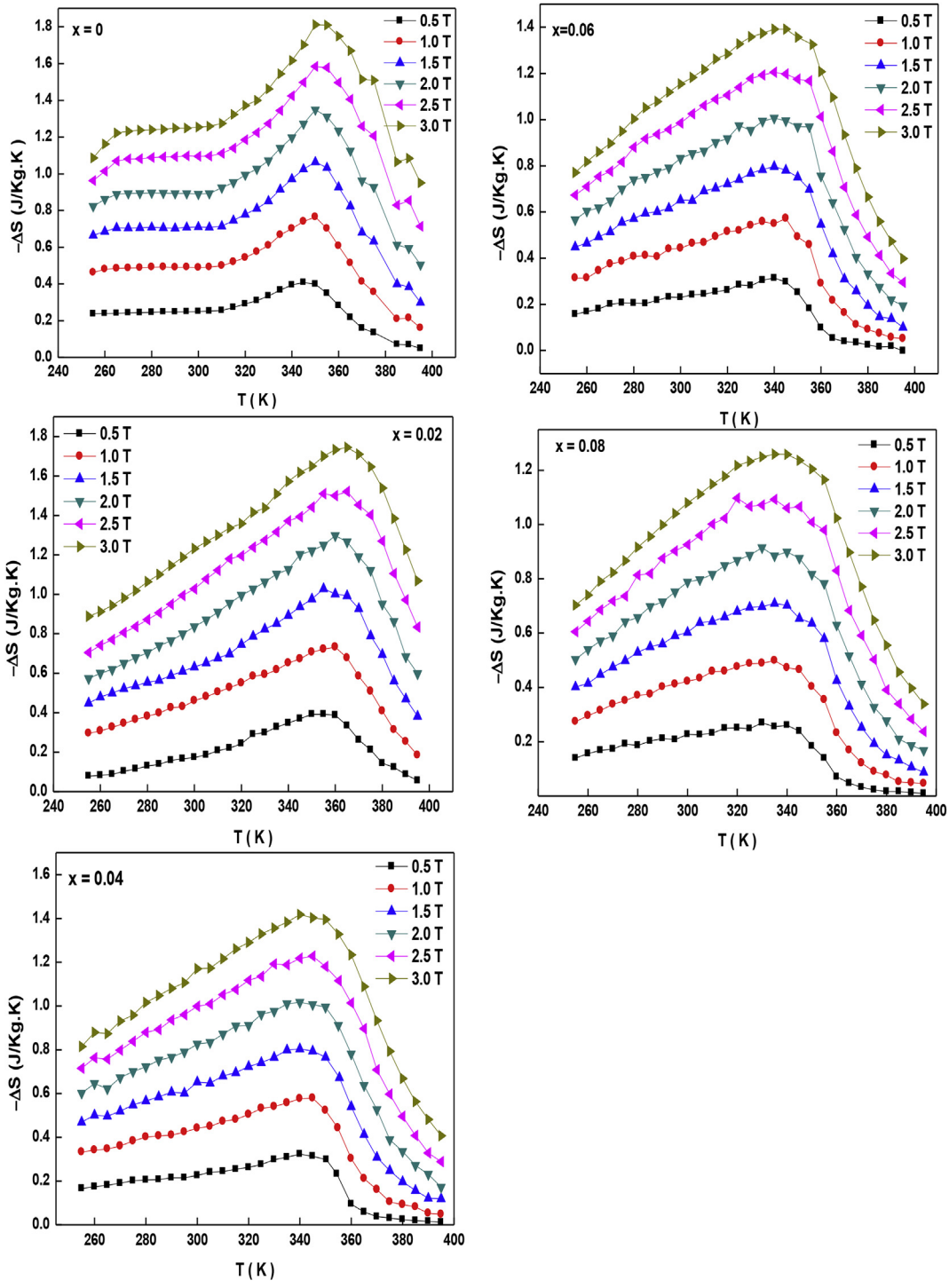

Fig. 10. Thermal variation of ΔS from 0 to 3T magnetic fields for LBMO/xTiO$_2$ composites.

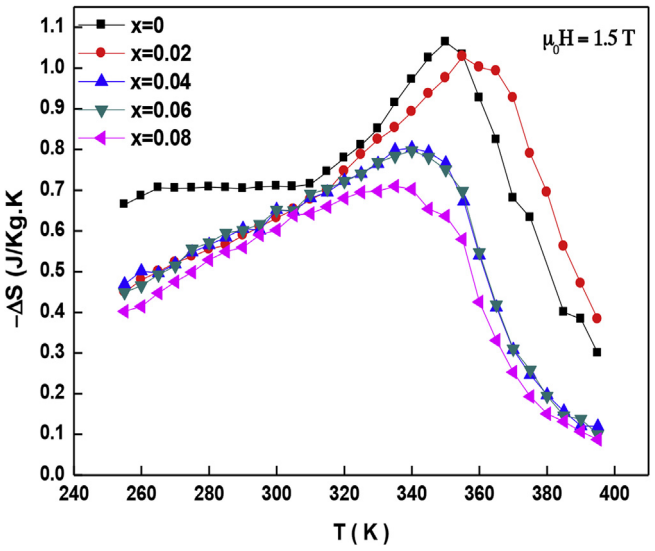

Fig. 11. ΔS dependent temperature as a function of doping level at 1.5T magnetic field.

Table 4
Comparison of magnetocaloric properties obtained in this work and reported results.

Compound	μ_0H (T)	T_c (K)	δT_{FWHM} (K)	RCP (J/Kg)	Ref
$La_{0.7}Ba_{0.3}MO_3$	1.5	348	32.91	35	This work
$La_{0.7}Ba_{0.3}MO_3/(TiO_2)_{0.02}$	1.5	348	50.02	51	This work
$La_{0.7}Ba_{0.3}MO_3/(TiO_2)_{0.04}$	1.5	348	58.97	47	This work
$La_{0.7}Ba_{0.3}MO_3/(TiO_2)_{0.06}$	1.5	348	63.26	50	This work
$La_{0.7}Ba_{0.3}MO_3/(TiO_2)_{0.08}$	1.5	346	68.49	49	This work
$La_{0.7}Sr_{0.3}MnO_3$	2	369	–	29	[47]
$La_{0.7}Pb_{0.3}MnO_3$	5	352	–	48	[48]
$La_{0.67}Sr_{0.33}MnO_3$	5	370	–	252	[49]
$La_{0.7}Sr_{0.3}Mn_{0.95}Fe_{0.05}O_3$	5	343	–	215	[50]

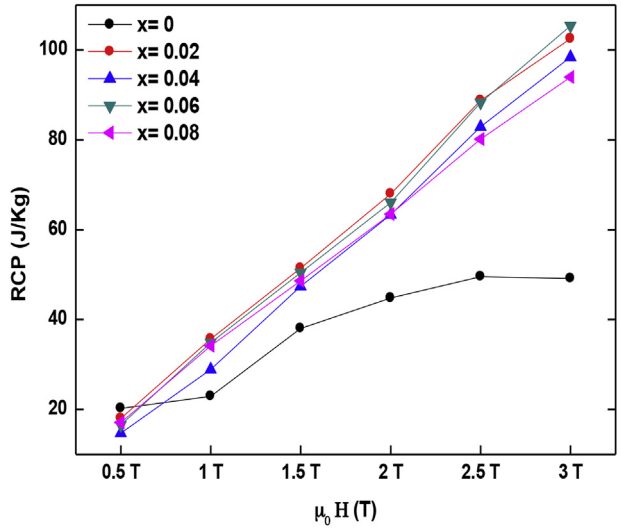

Fig. 12. RCP dependent magnetic fields for LBMO/xTiO$_2$ composites.

4. Conclusions

LBMO/xTiO$_2$ *manganite/insulator* system has been studied in composition range of $0 \leq x \leq 0.08$. XRD and SEM have proved the interaction lack between TiO_2 and LBMO in doped composites that keeps structure, cell volume and grain size without insignificant change. The LFMR peak of LBMO is shifted towards lower temperatures with TiO_2 doping and increases in value from −3% to −3.3, −3.5 and −3.7% for x = 0.02, 0.04 and 0.06. The TiO_2–LBMO interaction lack preserves the intrinsic properties of the LBMO system without any change with doping level as T_c. With respect to the magnetocaloric properties, the RCP values are enhanced with TiO_2 doping during the enhancement of the δT_{FWHM}. Where, the RCP of LBMO is enhanced from 35 J/kg to 51, 47, 49 and 50 J/kg for x = 0.02, 0.04, 0.06 and 0.08 doped composites at 1.5T magnetic field. In general, the good response of magnetoresistive and magnetocaloric properties of LBMO/xTiO$_2$ system in low magnetic fields may nominate these materials to be good potential candidates for both LFMR and magnetic refrigeration applications.

Acknowledgment

This work was financially supported by the Spanish Economy Department Ref. MAT201347231-C2-1-P and MAT2013-48054-C2-2-R, by the Asturias Government Ref. FC-15-GRUPIN14-085 research projects. Authors would like to acknowledge the Egyptian Ministry of Higher Education, technical and human support provided by SGIker Magnetic Measurements Gipuzkoa of UPV/EHU and by University of Oviedo SCT's.

References

[1] S. Jin, T.H. Tiefel, M. Mccormack, R.A. Fastnacht, R. Ramesh, L.H. Chen, Science 264 (1994) 413.
[2] S.K. Giri, P. Dasgupta, A. Poddar, T.K. Nath, J. Alloy. Compd. 631 (2015) 266.
[3] I. Bozovic, J.N. Eckstein, Appl. Surf. Sci. 113 (1997) 189.
[4] A.M. Ahmed, M.A. Abedellateef, H.A. Abd El-Ghanny, A.A. Mohamed, Phys. Status Solidi A 212 (2015) 623.
[5] S. Ricote, N. Bonanos, A. Manerbino, N.P. Sullivan, W.G. Coors, J. Mater. Chem. A 2 (2014) 16107.
[6] T.P. Pham, H.N. Luu, H.M. Do, D. T. h Tran, V.K. Nguyen, V.H. Le, X.P. Nguyen, Adv. Nat. Sci. Nanosci. Nanotechnol. 2 (2011) 025003.
[7] H. Hwang, S.W. Cheong, N.P. Ong, B. Batlogg, Phys. Rev. Lett. 77 (1996) 2041.
[8] K.A. Gschneidner Jr., V.K. Pecharsky, A.O. Tsokol, Rep. Prog. Phys. 68 (2005) 1479.
[9] A. Bouderbalaa, J.M. Chakroun, W.C. Koubaa, M. Koubaa, A. Cheikhrouhou, S. Nowak, S.A. Merah, Ceram. Int. 41 (2015) 7337.
[10] R. M'nassri, N.C. Boudjada, A. Cheikhrouhou, J. Alloy. Compd. 626 (2015) 20.
[11] V.K. Pecharsky, K.A. Gschneidner Jr., J. Magn. Magn. Mater 167 (1997) L179.
[12] V.K. Pecharsky, K.A. Gschneidner Jr., Phys. Rev. Lett. 78 (1997) 4494.
[13] J.C. Debnath, R. Zeng, J.H. Kim, S.X. Dou, J. Appl. Phys. 107 (2010) 09A916.
[14] V. Vega, M.A. Cerdeira, V.M. Prida, D. Alberts, N. Bordel, R. Pereiro, F. Mera, S. García, M.H. Vélez, M. Vázquez, J. Non-Cryst. Solids 354 (2008) 5233.
[15] X. Liu, J. Lin, Y.H. Tsang, X. Chen, P. Hing, H. Huang, J. Alloy. Compd. 607 (2014) 50.
[16] V. Sen, N. Panwar, A. Rao, C.K. Hsu, Y.K. Kuo, S.K. Agarwal, Solid State Commun. 145 (2008) 86.
[17] A. Barnabe, F. Millange, A. Maignan, M. Hervieu, B. Raveau, Chem. Mater. 10 (1998) 252.
[18] M.A.L. Quintela, L.E. Hueso, J. Rivas, F. Rivadulla, Nanotechnology 14 (2003) 212.
[19] B. Vertruyen, A. Rulmont, R. Cloots, M. Ausloos, S. Dorbolo, P. Vanderbemden, Mater. Lett. 57 (2002) 598.
[20] C. Zener, Phys. Rev. 81 (1951) 440.
[21] N. Zhang, W. Ding, W. Zhong, D. Xing, Y. Du, Phys. Rev. B 56 (1997) 8138.
[22] A.M. Ahmed, H.F. Mohamed, A.K. Diab, A.A. Mohamed, A.E.A. Mazen, A.M. Mohamed, Indian J. Phys. 89 (2015) 561.
[23] L.W. Lei, Z.Y. Fu, J.Y. Zhang, H. Wang, Mater. Sci. Eng. B 128 (2006) 70.
[24] B. x Huang, Y. h Liu, X. Yuan, C.J. Wang, R.Z. Zhang, L.M. Mei, J. Magn. Magn. Mater. 280 (2004) 176.
[25] A. de Andres, M.G. Hernandez, J.L. Martinez, Phys. Rev. B 60 (1999) 7328.
[26] L.E. Hueso, J. Rivas, F. Rivadulla, M.A.L. Quintela, J. Appl. Phys. 86 (1999) 3881.
[27] D. Das, C.M. Srivastava, D. Bahadur, A.K. Nigam, S.K. Malik, J. Phys. Condens. Mat. 16 (2004) 4089.
[28] N.F. Mott, E.A. Davis, Electronics Process in Non Crystalline Materials, second ed., Clarendon Press, Oxford, 1979.

[29] M. Viret, L. Ranno, J.M.D. Coey, Phys. Rev. B 55 (1997) 8067.
[30] S. Ravi, M. Kar, Phys. B 348 (2004) 169.
[31] N. Mahamdioua, A. Amira, S.P. Altintas, A. Varilci, C. Terzioglu, Phys. B 429 (2013) 12.
[32] A.M. Ahmed, A.A. Mohamed, M.A. Abdellateef, H.A. Abd El-Ghanny, Rare Met. (2015), http://dx.doi.org/10.1007/s12598-015-0465-x (in press).
[33] S. Gupta, R. Ranjit, C. Mitra, P. Raychaudhuri, R. Pinto, Appl. Phys. Lett. 78 (2001) 362.
[34] M. Eshraghi, H. Salamati, P. Kameli, J. Alloy. Compd. 437 (2007) 22.
[35] T.F. Zhou, G. Li, N.Y. Wang, B.M. Wang, X.G. Li, Y. Chen, Appl. Phys. Lett. 88 (2006) 232508.
[36] X.J. Liua, Z.Q. Lia, A. Yu, M.L. Liu, W.R. Li, B.L. Li, P. Wu, H.L. Bai, E.Y. Jiang, J. Magn. Magn. Mater. 313 (2007) 360.
[37] H.J. Kim, S.I. Yoo, J. Alloy. Compd. 521 (2012) 30.
[38] S. Karmakar, S. Taran, B.K. Chaudhuri, H. Sakata, C.P. Sun, C.L. Huang, H.D. Yang, J. Phys. D. Appl. Phys. 38 (2005) 3757.
[39] G. Venkataiah, P.V. Reddy, J. Magn. Magn. Mater. 285 (2005) 343.
[40] A. Dutta, N. Gayathri, R. Ranganathan, Phys. Rev. B 68 (2003) 054432.
[41] Y. Fu, Appl. Phys. Lett. 77 (2000) 118.
[42] S.K. Banerjee, Phys. Lett. 12 (1964) 67.
[43] V.S. Amaral, J.S. Amaral, J. Magn. Magn. Mater. 272 (2004) 2104.
[44] L.D. Landau, E.M. Lifshitz, Statistical Physics, third ed., Pergamon, Oxford, 1980.
[45] V.K. Pecharsky, K.A. Gschneidner Jr., J. Appl. Phys. 86 (1999) 565.
[46] J. Mira, J. Rivas, L.E. Hueso, F. Rivadulla, M.A.L. Quintela, J. Appl. Phys. 91 (2002) 8903.
[47] B. Arayedh, S. Kallel, N. Kallel, O. Peña, J. Magn. Magn. Mater. 361 (2014) 68.
[48] S.G. Min, K.S. Kim, S.C. Yu, H.S. Suh, S.W. Lee, IEEE Trans. Magn. 41 (2005) 2760.
[49] A. Rostamnejadi, M. Venkatesan, P. Kameli, H. Salamati, J.M.D. Coey, J. Magn. Magn. Mater. 323 (2011) 2214.
[50] S.K. Barik, C. Krishnamoorthi, R. Mahendiran, J. Magn. Magn. Mater. 323 (2011) 1015.